symmetry

MDPI

Article

Stochastic Characterization of MAC-Level Reliability and Reassociation Dynamics in IEEE 802.15.4 Networks for Smart Grid Applications

Carolina Del-Valle-Soto [1,*], José A. Del-Puerto-Flores [1], Ramiro Velázquez [2], Juan Sebastián Botero-Valencia [3], Leonardo J. Valdivia [1], José Varela-Aldás [4] and Paolo Visconti [5]

[1] Facultad de Ingeniería, Universidad Panamericana, Álvaro del Portillo 49, Zapopan 45010, Mexico; jpuerto@up.edu.mx (J.A.D.-P.-F.); lvaldivia@up.edu.mx (L.J.V.)
[2] Facultad de Ingeniería, Universidad Panamericana, Aguascalientes 20290, Mexico; rvelazquez@up.edu.mx
[3] Grupo Sistemas de Control y Robótica, Faculty of Engineering, Instituto Tecnológico Metropolitano, Medellin 050034, Colombia; juanbotero@itm.edu.co
[4] Centro de Investigación MIST, Facultad de Ingenierías, Universidad Tecnológica Indoamérica, Ambato 180103, Ecuador; josevarela@uti.edu.ec
[5] Department of Innovation Engineering, University of Salento, 73100 Lecce, Italy; paolo.visconti@unisalento.it
* Correspondence: cvalle@up.edu.mx

Abstract

Wireless communication networks based on IEEE 802.15.4 and ZigBee PRO constitute a critical component of smart grid infrastructures, where reliability and availability requirements exceed those typically assumed in low-power wireless deployments. Despite extensive analytical modeling, most existing studies rely on independence assumptions for packet errors and simplified abstractions of reassociation dynamics. This work presents stochastic reliability characterization grounded on real MAC-layer traffic capture from an operational IEEE 802.15.4/ZigBee PRO network. The methodology combines statistical hypothesis testing, first-order Markov modeling, spectral-gap analysis, large-deviation theory, renewal processes, and survival analysis of realignment intervals. Empirical results reject the hypothesis of independent frame errors and demonstrate significant temporal dependence with geometric mixing behavior. The estimated transition structure reveals burst-error persistence, inflating long-run variance relative to memoryless models. Furthermore, coordinator realignment intervals deviate from exponential behavior, exhibiting non-constant event rates consistent with regenerative dynamics. These findings indicate that effective communication reliability is governed not only by average frame error probability but also by dependence structure and regeneration mechanisms. The proposed probabilistic framework provides a rigorous and reproducible methodology for dependence-aware reliability assessment in smart grid communication systems.

Keywords: IEEE 802.15.4; ZigBee PRO; smart grid communications; MAC-layer reliability; Markov chains; temporal dependence; renewal processes; large deviations

Academic Editors: Jie Yang, Chong Wang and George Karabatsos

Received: 4 March 2026
Revised: 24 March 2026
Accepted: 31 March 2026
Published: 14 April 2026

1. Introduction

Wireless communication technologies based on IEEE 802.15.4 and ZigBee PRO are a fundamental component of smart grid infrastructure, particularly in Advanced Metering Infrastructure (AMI) [1], Home Area Networks (HAN), and distributed energy resource monitoring systems. These networks are expected to operate under stringent reliability and availability constraints while maintaining low power consumption and scalability [2].

Despite their widespread deployment, most existing performance evaluations rely on analytical abstractions or simulation-based studies that assume independent and identically distributed (i.i.d.) packet error processes and stationary channel conditions. Such assumptions, while analytically convenient, remain insufficiently validated under real traffic conditions representative of operational smart grid environments [3].

Beyond their functional role in distributed monitoring and metering, low-power wireless networks embedded in smart grid infrastructures constitute stochastic dynamical systems whose reliability properties emerge from the interaction between medium access control, channel variability [4–7], and network-layer coordination mechanisms. From a theoretical standpoint, reliability in such systems is not merely a function of average packet error probability, but rather of the temporal structure of errors, correlation decay, and regeneration phenomena. In applied probability terms, communication reliability becomes a problem of characterizing additive functionals of dependent stochastic processes under finite-energy and finite-latency constraints. This perspective connects smart grid communication analysis with ergodic theory, renewal processes, and large deviation principles, which have long provided the mathematical foundation for reliability modeling in complex engineered systems [8,9].

In practical smart grid deployments, communication subsystems operate under heterogeneous traffic loads, time-varying interference in unlicensed bands, and dynamic topology reconfiguration [10]. These factors induce burst-error behavior and non-stationary dynamics that cannot be adequately captured by memoryless abstractions. Empirical studies in wireless sensor and industrial networks have demonstrated that temporal correlation in packet loss significantly alters queueing performance, energy consumption, and latency distributions [11,12]. In safety-critical infrastructures, short-range dependence alone can inflate variance and increase the probability of threshold violations, even when average error rates remain within nominal limits. Consequently, rigorous reliability assessment requires dependence-aware asymptotic inference and spectral analysis rather than purely mean-based metrics.

From a broader systems perspective, smart grid communication reliability must also be interpreted through the lens of resilience and stochastic stability. Modern grid architectures increasingly integrate distributed energy resources, demand–response mechanisms, and cyber–physical feedback loops, thereby coupling communication performance with physical-layer stability [13,14]. In such environments, intermittent communication degradation may propagate into control-layer oscillations or delayed corrective actions. Theoretical constructs such as regenerative processes, mixing coefficients, and large deviation rate functions offer a principled way to quantify these risks and to distinguish between benign fluctuations and structurally destabilizing regimes. Embedding communication reliability within this stochastic-systems framework is therefore essential for advancing both theoretical understanding and operational robustness in smart grid infrastructures [15].

A complementary perspective on smart grid communication reliability arises from the increasing integration of heterogeneous wireless technologies and multi-hop architectures, which introduce additional layers of stochastic variability beyond single-link behavior [16]. In particular [17], mesh-based IEEE 802.15.4 deployments and hybrid IoT—smart grid environments exhibit complex interactions between routing protocols, interference patterns, and duty-cycling mechanisms, leading to non-trivial spatiotemporal correlation structures in packet delivery processes. Recent experimental and modeling studies have shown that cross-layer interactions between MAC contention, routing dynamics, and energy-saving strategies can significantly affect reliability and latency distributions [18], especially under dense network conditions or coexistence with other wireless systems operating in the same ISM band [16,19,20]. These findings highlight the need to move beyond isolated

link-level analysis toward integrated stochastic models that capture both temporal and network-level dependencies.

In addition, the growing adoption of data-driven and measurement-based methodologies in communication network analysis has enabled more accurate characterization of real-world wireless behavior. Unlike traditional analytical models [21], which often rely on simplifying assumptions for tractability, empirical approaches leverage large-scale traffic traces and experimental testbeds to reveal hidden structures such as error bursts, non-stationarity, and context-dependent performance regimes. In the context of low-power wireless networks, measurement-driven studies have demonstrated that environmental factors [22], interference sources, and protocol dynamics jointly induce variability patterns that are not captured by classical models [23,24]. This shift toward empirical stochastic modeling is particularly relevant for smart grid applications, where reliability requirements are stringent, and model inaccuracies may translate into operational risks [25].

1.1. Motivation

Despite these advances, a fundamental research gap remains in the reliability characterization of IEEE 802.15.4 smart grid communication systems.

Existing Markov-based models in wireless sensor networks and industrial IoT typically rely on analytically constructed state transitions or simulated traffic, without empirical validation using real MAC-layer traces. As a result, key properties such as transition asymmetry, burst-error persistence, and correlation structure are often assumed rather than inferred from measurements. In parallel, smart grid communication studies frequently adopt independence assumptions or simplified reliability abstractions that do not account for temporal dependence in packet errors. Even when Markov models are employed, they are rarely derived from real traffic data and are not accompanied by formal statistical testing of independence or mixing behavior.

Furthermore, dynamic network events such as coordinator realignment and reassociation are commonly treated as deterministic or exogenous processes, without being modeled as stochastic regeneration mechanisms with measurable inter-event distributions. Consequently, there is a lack of empirically grounded, dependence-aware stochastic frameworks that jointly capture error dynamics, temporal correlation, and reassociation behavior in real IEEE 802.15.4 smart grid deployments.

This paper addresses this gap through a stochastic reliability characterization of an IEEE 802.15.4/ZigBee PRO network based on an extensive real-world traffic capture. The dataset includes MAC data frames, data request commands, acknowledgment frames, coordinator realignment messages, orphan notifications, and ZigBee PRO beacons observed over a prolonged measurement interval. A significant proportion of captured frames exhibit Frame Check Sequence (FCS) errors, thereby enabling empirical investigation of MAC-layer failure dynamics. Rather than treating transmission errors as memoryless events, this work rigorously evaluates temporal dependence structures and reassociation dynamics, developing a probabilistic framework that reflects the intrinsic behavior of real IEEE 802.15.4 smart grid communications.

The novelty of this study lies in grounding the stochastic model directly on empirical MAC-layer observations and in formally testing independence assumptions commonly adopted in the literature. The resulting model provides not only statistical characterization but also interpretable reliability metrics directly translatable into smart grid performance indicators such as availability, Mean Time Between Failures (MTBF), and stability under reassociation events.

Application Context in Smart Grid Systems

The analyzed IEEE 802.15.4/ZigBee PRO network can be interpreted as a representative instance of an Advanced Metering Infrastructure (AMI) communication subsystem. In this scenario, the coordinator operates as a data concentrator, while the end devices emulate smart meters, periodically requesting consumption data and network updates.

This traffic pattern, characterized by periodic polling combined with asynchronous control signaling, is consistent with real-world AMI deployments in which smart meters communicate with a central unit over low-power wireless links. The observed reassociation events correspond to network maintenance operations such as re-synchronization, orphan recovery, or topology adjustment, which are critical for ensuring long-term system availability.

Within this application context, the stochastic properties identified in this work acquire direct operational meaning. Burst-error persistence, as captured by the transition probability $\widehat{p}_{11}$, translates into consecutive transmission failures that may increase latency and retransmission overhead. The spectral gap quantifies the rate at which adverse communication conditions dissipate, thereby providing a measure of resilience to transient disturbances. Furthermore, the non-exponential distribution of realignment intervals reflects state-dependent instability mechanisms that impact long-term availability and Mean Time Between Failures (MTBF).

By explicitly linking empirical measurements to an AMI communication scenario, the proposed stochastic framework provides reliability metrics that are directly interpretable in terms of smart grid performance requirements, including data delivery reliability, temporal stability, and resilience under network reconfiguration events.

The remainder of this paper is organized as follows. Section 2 reviews the relevant literature on IEEE 802.15.4 reliability modeling, smart grid communication performance, and stochastic process approaches to dependent error dynamics. Section 3 describes the captured dataset and presents the statistical inference and stochastic modeling framework, including independence testing, Markov chain estimation, large-deviation analysis, and regenerative modeling of realignment events. Section 4 reports the empirical results, including spectral analysis, variance inflation under dependence, survival modeling of reassociation intervals, and asymptotic behavior of the empirical error rate. Section 5 discusses the implications of the findings for reliability assessment and system-level stability. Finally, Section 6 concludes the paper and outlines directions for future research.

2. Related Work

Analytical modeling of IEEE 802.15.4 networks has continued to evolve in recent years, primarily focusing on CSMA/CA backoff dynamics, contention probability, delay performance, and throughput optimization under saturated and unsaturated traffic conditions. Several works extend Bianchi-type discrete-time Markov chain formulations to characterize medium access behavior and collision probability in low-power wireless networks deployed in smart grid scenarios [26,27]. These studies provide steady-state performance metrics, such as throughput, delay, and packet delivery ratio, typically under the assumption of independent transmission attempts and stationary traffic-generating processes.

At the physical layer, packet error probability is commonly derived under additive white Gaussian noise (AWGN) or Rayleigh fading models, often assuming temporal independence of channel realizations. While such assumptions enable tractable closed-form expressions, they abstract from burst-error phenomena induced by interference, multipath fading, or correlated contention. Recent reliability-oriented studies in industrial and sensor networks have highlighted that correlated failures significantly impact performance metrics

and reliability bounds [28,29]. However, most analyses remain state-based and do not incorporate empirical dependence estimation from real MAC-layer traces.

In the context of smart grid communication systems, research has largely emphasized latency guarantees, queueing performance, and network-level reliability modeling [30,31]. Survey contributions have identified communication reliability as a critical enabler of grid stability and resilience [32], yet empirical stochastic characterization of MAC-layer error dynamics remains limited. Existing smart grid reliability models often assume independence or employ finite-state abstractions without formally testing for temporal dependence in measured traffic.

Markov reliability modeling has been employed to capture correlated component failures in wireless sensor and industrial IoT systems [28,33]. These works demonstrate that dependence structures alter steady-state reliability and variance properties, but typically rely on synthetic or simulated data rather than real captured MAC-layer traces. Similarly, resilience analyses of smart grid communication infrastructures often employ conceptual or simulation-based frameworks without grounding stochastic assumptions in empirical observations [18].

A further methodological limitation concerns dynamic reassociation and coordinator realignment mechanisms in ZigBee PRO networks. Although delay and reliability analyses of ZigBee-based smart grid deployments have been reported [27], reassociation events are usually treated deterministically or incorporated as exogenous disruptions rather than modeled as stochastic regeneration phenomena. The renewal-theoretic structure induced by realignment cycles and its impact on long-run availability metrics have not been rigorously quantified in the recent literature.

From a stochastic-process perspective, modern treatments of regenerative processes, large deviations, and dependence-adjusted asymptotics provide the theoretical tools required for such analysis. However, their application to empirical IEEE 802.15.4 smart grid traffic remains scarce.

The present work advances the state-of-the-art by combining real MAC-layer traffic capture with formal statistical inference and stochastic-process modeling. Unlike prior studies that assume memoryless packet errors, we explicitly test independence, estimate Markov transition dynamics, quantify spectral-gap-driven mixing behavior, and evaluate large-deviation risk of reliability degradation. Furthermore, we model coordinator realignment events as regeneration points, thereby embedding smart grid communication reliability within a rigorous renewal-theoretic framework grounded in empirical data.

A structured comparison with existing literature is provided in Table 1.

Table 1. Critical comparison of representative studies addressing reliability modeling in IEEE 802.15.4, wireless sensor networks, and smart grid communication systems.

Reference	Modeling Scope	Empirical Validation	Temporal Dependence Modeling	Rare-Event/Tail Analysis	Stochastic-Process Rigor
Wijetunge et al. (2013) [26]	IEEE 802.15.4 MAC performance	No	No (independence assumed)	No	Steady-state Markov modeling
Alqahtani et al. (2021) [27]	ZigBee MAC delay analysis	No	No	No	Deterministic + Markov contention
Catelani et al. (2021) [34]	WSN reliability overview	Partial (testbeds)	No formal dependence analysis	No	Descriptive evaluation
Islam et al. (2012) [35]	Industrial wireless reliability	Yes (industrial scenarios)	Qualitative discussion	No	No inferential stochastic modeling
Baimel et al. (2016) [32]	Smart grid communication survey	No	Not addressed	No	Conceptual review
Shahabinejad et al. (2019) [33]	WSN reliability modeling	No	No	No	Markov reliability states
Gao et al. (2019) [29]	Industrial WSN reliability	Partial	Limited dependence modeling	No	State-based reliability analysis
Al-Khatib et al. (2020) [30]	Smart grid network performance	No	No	No	Queueing-level analysis
Li et al. (2022) [31]	Smart grid latency modeling	No	No	No	Descriptive + simulation-based
Liu et al. (2021) [28]	Markov reliability in WSN	No	Yes (finite-state)	No	Classical Markov reliability
Zuo et al. (2020) [36]	Industrial IoT reliability	Partial	Limited	No	Reliability block diagrams
Tsado et al. (2015) [18]	Smart grid resilience modeling	No	No	No	Qualitative resilience metrics
Asmussen & Glynn (2021) [37]	Renewal and regenerative processes	Theoretical	Yes	Yes (renewal asymptotics)	Rigorous applied probability
This Work	IEEE 802.15.4 MAC reliability under smart grid traffic	Yes (real MAC-layer capture)	Yes (Markov + mixing analysis)	Yes (large deviations + spectral analysis)	Ergodicity, renewal theory, long-run variance, CLT under dependence

3. Materials and Methods

The analyzed dataset consists of a real IEEE 802.15.4/ZigBee PRO traffic capture operating in the 2.4 GHz ISM band on Channel 11. The observed network architecture includes a coordinator node and multiple end devices periodically issuing MAC-level data requests. The traffic trace spans several thousand seconds of operation and contains heterogeneous frame types, including data transmissions, acknowledgments, beacons, coordinator realignment commands, and orphan notifications. Importantly, a substantial subset of frames is marked with FCS errors, indicating corrupted transmissions at the MAC layer.

3.1. Notation

For clarity and to facilitate readability, Table 2 summarizes the main mathematical symbols and notation used throughout the manuscript. The table provides a concise reference for the stochastic variables, model parameters, and key quantities involved in the probabilistic framework, enabling easier interpretation of the subsequent analysis.

Table 2. Mathematical symbols and notations used in the stochastic modeling framework.

Symbol	Description
N	Total number of observed MAC frames
N_e	Number of frames with FCS errors
E_i	Binary error indicator for frame i ($1 =$ error, $0 =$ success)
$\{E_i\}$	Sequence of MAC-layer transmission outcomes
$\widehat{\text{FER}}$	Empirical Frame Error Rate
p	Bernoulli error probability under independence assumption
$\mathbf{P}$	Transition matrix of the Markov chain
p_{ij}	Transition probability from state i to state j
$\widehat{p}_{ij}$	Estimated transition probability
$\boldsymbol{\pi}$	Stationary distribution of the Markov chain
π_1	Stationary error probability
λ_2	Second eigenvalue of the transition matrix
δ	Spectral gap ($\delta = 1 - \lvert\lambda_2\rvert$)
$\gamma(k)$	Autocovariance at lag k
σ^2	Long-run variance of the error process
Λ	Likelihood ratio test statistic
AIC, BIC	Information criteria for model selection
S_N	Partial sum $\sum_{i=1}^{N} E_i$
$I(a)$	Large deviation rate function
τ_k	Time of the k-th realignment event
C_k	Length of the k-th regeneration cycle
β, η	Weibull shape and scale parameters
$\lambda(t)$	Hazard (failure) rate function
A	Network availability
MTBF	Mean time between failures

3.2. Dataset Description and Preprocessing

The analyzed traffic trace was captured over a total duration of approximately $T = 3600$ s (1 h) under continuous network operation. The capture was performed on IEEE 802.15.4 Channel 11 (2.405 GHz) using a passive monitoring setup capable of recording all observable MAC-layer frames within radio range.

The network topology consists of a single ZigBee PRO coordinator and $M = 12$ end devices operating in a star-like configuration typical of smart grid Advanced Metering Infrastructure (AMI) deployments. End devices periodically generate MAC data request

commands to retrieve buffered data from the coordinator, resulting in quasi-periodic traffic patterns with additional asynchronous control signaling.

The captured traffic includes multiple frame types defined by the IEEE 802.15.4 standard, including data frames, Acknowledgment (ACK) frames, beacon frames, coordinator realignment commands, and orphan notifications. This heterogeneity enables joint analysis of reliability and reassociation dynamics.

3.2.1. Traffic Characteristics

Traffic generation is predominantly periodic, driven by application-layer polling mechanisms, with inter-request intervals ranging from approximately 1 to 5 s depending on device configuration. Background traffic includes acknowledgment exchanges and network maintenance signaling, producing a mixture of deterministic and stochastic temporal structures.

3.2.2. Identification of Corrupted Frames

Frame integrity is assessed using the Frame Check Sequence (FCS) field provided at the MAC layer. Frames flagged with invalid FCS values are classified as corrupted transmissions. These events are interpreted as transmission failures and encoded as $E_i = 1$ in the binary error sequence defined in (1). Frames with valid FCS are classified as successful transmissions ($E_i = 0$).

3.2.3. Interpretation of FCS Errors

It is important to note that FCS errors are detected at the monitoring device performing passive capture and therefore correspond to decoding failures at that receiver. As such, they do not necessarily imply that the original transmission failed at the intended destination node.

In wireless environments, spatial variations in channel conditions, interference, and receiver sensitivity may result in discrepancies between what the monitoring device observes and what network nodes successfully receive. Consequently, FCS errors should be interpreted as observable indicators of channel impairment and communication instability, rather than direct measurements of end-to-end packet delivery failure.

Within this work, the binary error sequence is therefore understood as a receiver-side reliability proxy that captures temporal variations in channel quality and network conditions, which are the primary focus of the stochastic analysis.

3.2.4. Preprocessing Pipeline

The raw packet capture undergoes preprocessing before stochastic analysis. This includes the following:

- Filtering of non-IEEE 802.15.4 frames and malformed packets.
- Chronological ordering of frames based on timestamp to ensure temporal consistency.
- Extraction of MAC-layer metadata, including frame type and FCS status.
- Construction of the binary error sequence $\{E_i\}_{i=1}^{N}$ used for statistical inference.
- Identification of realignment events and computation of inter-event intervals for survival analysis.

3.2.5. Identification of Realignment Events

Coordinator realignment events are explicitly identified from the MAC-layer trace based on IEEE 802.15.4 frame-type and command-field inspection. In particular, frames classified as coordinator realignment commands are detected using their MAC command iden-

tifier, as defined in the IEEE 802.15.4 standard. Additionally, orphan notification messages followed by coordinator responses are used to corroborate reassociation-related transitions.

A total of $N_r = 47$ realignment events were identified over the observation interval of $T = 3600$ s. Each event timestamp τ_k is defined as the reception time of a coordinator realignment command or the first frame in a reassociation sequence.

To ensure robustness, consecutive control frames occurring within a short temporal window (less than 1 s) are grouped and treated as a single realignment event. This avoids overcounting protocol-level retransmissions or closely spaced signaling bursts.

The resulting sequence $\{\tau_k\}$ is used to construct inter-event intervals $C_k = \tau_{k+1} - \tau_k$, which form the basis for the renewal and survival analyses presented in subsequent sections.

3.2.6. Treatment of Malformed Packets

Malformed packets, defined as frames that do not conform to the IEEE 802.15.4 MAC frame structure or lack valid decoding at the physical layer, are excluded from the analysis. These packets are not incorporated into the binary error sequence $\{E_i\}_{i=1}^{N}$, as they do not provide reliable information regarding transmission outcomes.

The construction of the stochastic process is therefore restricted to well-formed MAC frames with valid structural fields. Among these, classification into successful or failed transmissions is based exclusively on FCS validation, as described previously. This ensures that the binary sequence reflects only meaningful transmission events and avoids bias introduced by incomplete or undecodable packets.

No imputation or smoothing is applied to the data; the analysis is performed directly on the observed sequence to preserve the intrinsic temporal dependence structure.

This detailed characterization ensures that the dataset and preprocessing methodology are fully transparent and reproducible, thereby supporting the validity of the subsequent stochastic modeling framework.

3.2.7. Dataset

For reproducibility, we summarize the key characteristics of the analyzed dataset. The capture consists of a total of $N = 52{,}846$ IEEE 802.15.4 MAC frames collected over a duration of $T = 3600$ s under continuous operation. Among these, $N_e = 17{,}392$ frames are identified as corrupted based on FCS validation.

The network comprises $M = 12$ end devices and one coordinator, arranged in a star topology, consistent with a smart grid Advanced Metering Infrastructure (AMI) deployment. End devices emulate smart meters issuing periodic data requests to the coordinator, which acts as a data concentrator.

The capture setup is passive and channel-specific (Channel 11, 2.405 GHz), ensuring that all observable MAC-layer activity within radio range is recorded without influencing network operation. The resulting dataset contains a heterogeneous mixture of data, acknowledgment, beacon, and control frames, enabling joint analysis of reliability and reassociation dynamics. This consolidated description complements the detailed preprocessing pipeline and ensures that the dataset and experimental conditions are fully transparent and reproducible.

3.2.8. Deployment Environment and Interference Conditions

The analyzed dataset was obtained under real operating conditions in an indoor environment representative of a smart grid laboratory testbed. The network operated in the 2.4 GHz ISM band, which is shared with other wireless technologies such as WiFi (IEEE 802.11) and Bluetooth [38]. Consequently, the communication channel was subject to uncontrolled external interference and background traffic from coexisting wireless systems.

Although no active interference was generated during capture, the passive monitoring setup inherently reflects realistic channel conditions, including temporal fluctuations in interference levels, multipath propagation, and medium contention. These factors contribute to variability in frame reception quality and are consistent with typical deployment scenarios of IEEE 802.15.4 networks in urban or industrial environments.

3.2.9. Measurement Scope and Limitations

It is important to emphasize that the dataset corresponds to a single deployment scenario with a fixed network configuration and operating conditions. While the sample size is sufficiently large to support statistical inference, the results should be interpreted within the context of the analyzed environment. In particular, variations in interference intensity, node density, traffic load, or physical layout may lead to different quantitative results in other deployments.

Therefore, the dataset provides an empirically grounded but scenario-specific characterization of MAC-layer reliability, which is suitable for dependence analysis but does not aim to represent all possible IEEE 802.15.4 smart grid configurations.

Let $N \in \mathbb{N}$ denote the total number of observed MAC frames in the captured IEEE 802.15.4 traffic trace. For each frame index $i \in \{1, 2, \ldots, N\}$, we define the binary random variable E_i as

$$E_i = \begin{cases} 1, & \text{if the } i\text{-th frame contains a Frame Check Sequence (FCS) error,} \\ 0, & \text{otherwise.} \end{cases} \tag{1}$$

We formalize the error sequence as a stochastic process defined on a probability space $(\Omega, \mathcal{F}, \mathbb{P})$. Specifically,

$$E : \Omega \times \mathbb{N} \to \{0, 1\}, \tag{2}$$

such that $E_i(\omega) = E(\omega, i)$ represents the outcome of the i-th frame transmission.

The natural filtration associated with the process is defined as

$$\mathcal{F}_n = \sigma(E_1, E_2, \ldots, E_n), \tag{3}$$

which represents the information available up to frame n.

This formalization allows subsequent derivations concerning ergodicity, mixing properties, and asymptotic convergence.

The stochastic process $\{E_i\}_{i=1}^{N}$ therefore represents the sequence of MAC-layer transmission outcomes, where $E_i = 1$ indicates a corrupted frame and $E_i = 0$ denotes a correctly received frame. Equation (1) formally encodes the frame-level reliability indicator used throughout the subsequent probabilistic analysis.

The empirical Frame Error Rate (FER), defined as the sample mean of the binary error process, is estimated as

$$\widehat{\mathrm{FER}} = \frac{1}{N} \sum_{i=1}^{N} E_i. \tag{4}$$

The estimator in (4) corresponds to the maximum likelihood estimator of the Bernoulli error probability under the assumption of independent and identically distributed transmission outcomes. In subsequent sections, this estimator will serve as the baseline reliability metric against which more structured stochastic models, such as Markov-dependent formulations, will be compared.

In addition to frame-level error indicators, temporal information is extracted to compute inter-arrival times, reassociation intervals, and the distribution of data request sequences. Coordinator realignment and orphan notification events are treated as state-

transition triggers affecting network stability. The resulting dataset thus permits both pointwise error analysis and temporal stochastic modeling.

Under the i.i.d. Bernoulli assumption in (2), the estimator in (4) satisfies

$$\mathbb{E}[\widehat{\mathrm{FER}}] = p, \qquad \mathrm{Var}(\widehat{\mathrm{FER}}) = \frac{p(1-p)}{N}. \tag{5}$$

By the strong law of large numbers,

$$\widehat{\mathrm{FER}} \xrightarrow{a.s.} p \quad \text{as } N \to \infty, \tag{6}$$

and by the central limit theorem,

$$\sqrt{N}\left(\widehat{\mathrm{FER}} - p\right) \xrightarrow{d} \mathcal{N}(0, p(1-p)). \tag{7}$$

If temporal dependence exists, the asymptotic variance must instead be expressed as

$$\sigma^2 = \gamma(0) + 2\sum_{k=1}^{\infty} \gamma(k), \tag{8}$$

where $\gamma(k) = \mathrm{Cov}(E_i, E_{i+k})$ denotes the autocovariance function.

3.3. Statistical Inference and Stochastic Modeling Framework

The methodological framework is grounded in statistical inference and stochastic process modeling applied to the binary error sequence $\{E_i\}_{i=1}^{N}$ defined in (1). The first stage of the analysis evaluates whether the observed process can be adequately described as an independent and identically distributed (i.i.d.) Bernoulli sequence.

Under the null hypothesis of independence, each frame outcome is assumed to follow

$$E_i \sim \mathrm{Bernoulli}(p), \tag{9}$$

where $p \in (0,1)$ denotes a constant frame error probability. The corresponding null and alternative hypotheses are formulated as

$$H_0 : \{E_i\} \text{ is an i.i.d. Bernoulli process with parameter } p, \tag{10}$$

$$H_1 : \{E_i\} \text{ exhibits temporal dependence.} \tag{11}$$

Independence is evaluated using the Wald–Wolfowitz runs test, the sample Autocorrelation Function (ACF), and the Ljung–Box portmanteau statistic applied to the binary sequence. Rejection of H_0 in (10) implies that the error process exhibits statistically significant temporal dependence, thereby invalidating the memoryless assumption embedded in (9).

3.4. First-Order Markov Chain Modeling

If independence is rejected, the sequence $\{E_i\}$ is modeled as a first-order discrete-time Markov chain with state space

$$\mathcal{S} = \{0, 1\}, \tag{12}$$

where state 0 represents a correctly received frame and state 1 represents a frame with FCS error.

The transition probability matrix is defined as

$$\mathbf{P} = \begin{pmatrix} p_{00} & p_{01} \\ p_{10} & p_{11} \end{pmatrix}, \tag{13}$$

where

$$p_{ij} = \mathbb{P}(E_{n+1} = j \mid E_n = i), \quad i, j \in \mathcal{S}. \tag{14}$$

Maximum likelihood estimation of the transition probabilities in (14) is obtained from observed transition counts N_{ij} as follows:

$$\widehat{p}_{ij} = \frac{N_{ij}}{\sum_{j \in \mathcal{S}} N_{ij}}, \tag{15}$$

provided $\sum_j N_{ij} > 0$.

Model adequacy is evaluated by comparing the likelihood of the Bernoulli model (9) with that of the Markov chain defined by (13). The likelihood ratio statistic is computed as

$$\Lambda = -2 \log \left(\frac{L_{\text{Bernoulli}}}{L_{\text{Markov}}} \right), \tag{16}$$

and it is asymptotically χ^2-distributed under standard regularity conditions. Additionally, model selection is supported through information-theoretic criteria, namely the Akaike Information Criterion (AIC) and Bayesian Information Criterion (BIC),

$$\text{AIC} = -2 \log L + 2k, \tag{17}$$

$$\text{BIC} = -2 \log L + k \log N, \tag{18}$$

where k denotes the number of estimated parameters and L the maximized likelihood.

The stationary distribution $\boldsymbol{\pi} = (\pi_0, \pi_1)$ of the Markov chain is obtained by solving

$$\boldsymbol{\pi} \mathbf{P} = \boldsymbol{\pi}, \quad \text{subject to} \quad \pi_0 + \pi_1 = 1. \tag{19}$$

The stationary error probability π_1 provides an estimate of the long-run frame error probability under dependent dynamics and allows comparison with the empirical estimator in (4). Convergence properties are assessed through eigenvalue analysis of $\mathbf{P}$.

The Markov chain defined by (13) is irreducible if and only if

$$p_{01} > 0 \quad \text{and} \quad p_{10} > 0. \tag{20}$$

It is aperiodic provided

$$p_{00} > 0 \quad \text{and} \quad p_{11} > 0. \tag{21}$$

Under irreducibility and aperiodicity, the chain is ergodic and converges to its stationary distribution:

$$\lim_{n \to \infty} \mathbf{P}^n = \begin{pmatrix} \pi_0 & \pi_1 \\ \pi_0 & \pi_1 \end{pmatrix}. \tag{22}$$

Let $\lambda_1 = 1$ and λ_2 denote the eigenvalues of $\mathbf{P}$. The second eigenvalue satisfies

$$\lambda_2 = p_{00} + p_{11} - 1. \tag{23}$$

The spectral gap,

$$\delta = 1 - |\lambda_2|, \tag{24}$$

governs the rate of geometric convergence to stationarity and characterizes burst persistence in the error process.

3.4.1. Significance Levels and Decision Criteria

All statistical tests are conducted using a significance level of $\alpha = 0.05$. The null hypothesis of independence in (10) is rejected whenever the corresponding p-value is strictly less than α.

For the Wald–Wolfowitz runs test, rejection occurs if the standardized statistic falls in the critical region associated with α, equivalently when the reported p-value satisfies $p < \alpha$. For the Ljung–Box test, the null hypothesis of no autocorrelation up to lag k is rejected when the test statistic exceeds the χ^2 critical value with k degrees of freedom, or equivalently when $p < \alpha$.

Similarly, for the likelihood ratio test in (16), the Bernoulli model is rejected in favor of the Markov model when the test statistic exceeds the corresponding χ^2 threshold or when the associated p-value is below α.

All reported results satisfy $p < 10^{-6}$, providing strong statistical evidence against the null hypothesis of independence.

3.4.2. Justification of First-Order Markov Assumption

The adoption of a first-order Markov model is motivated by both empirical evidence and model parsimony considerations. To assess whether higher-order dependence is present, we examined conditional transition probabilities of the following form:

$$\mathbb{P}(E_{n+1} = 1 \mid E_n = i, E_{n-1} = j), \quad i, j \in \{0, 1\},$$

and compared them with the first-order probabilities $\mathbb{P}(E_{n+1} = 1 \mid E_n = i)$.

The empirical estimates showed that conditioning on E_{n-1} produces only marginal changes relative to the first-order transition probabilities, indicating that most of the dependence structure is captured by the immediate past state. This observation is consistent with the rapidly decaying autocovariance function $\gamma(k)$ and the geometric mixing behavior reported in the Results section.

To further validate this choice, we compared first- and second-order Markov models using likelihood-based criteria. The second-order model increases the number of parameters without yielding a substantial improvement in likelihood, and is penalized by both AIC and BIC. This indicates that the additional complexity is not justified by the available data. From a stochastic-process perspective, the presence of a strictly positive spectral gap and geometric decay of correlations implies short-range dependence, for which a first-order Markov approximation provides an adequate and parsimonious representation. Therefore, the first-order Markov model captures the dominant temporal dependence in the MAC-layer error process while avoiding overparameterization and ensuring statistical robustness.

3.4.3. Interpretation in Terms of Burst-Error Modeling

An important advantage of the first-order Markov model over the independent Bernoulli model lies in its ability to explicitly capture burst-error behavior. Under the i.i.d. assumption, the probability of observing consecutive transmission failures is given by p^k, which decreases exponentially with the length k of the error sequence. This implies that long error bursts are extremely unlikely.

In contrast, the Markov model introduces state-dependent transition probabilities, allowing the probability of consecutive errors to be governed by the persistence parameter p_{11}. In particular, the probability of a burst of length k is approximately $p_{11}^{k-1}p_{10}$, which decays at a rate determined by p_{11}. When p_{11} is large, as observed in the empirical results, the model assigns significantly higher probability to consecutive failures than the Bernoulli model.

This structural difference explains the Markov model's ability to reproduce the observed clustering of transmission errors and to capture variance-inflation effects through its autocovariance structure. Consequently, the first-order Markov formulation provides a minimal yet sufficient extension of the independent model that incorporates temporal dependence while preserving analytical tractability.

3.5. Large Deviations of the Empirical Error Rate

Beyond asymptotic normality, we examine rare-event behavior of the empirical error rate.

Under the i.i.d. Bernoulli model, Cramér's theorem implies

$$\mathbb{P}(\widehat{\mathrm{FER}} \geq a) \approx \exp(-NI(a)), \tag{25}$$

where the rate function is

$$I(a) = a \log\left(\frac{a}{p}\right) + (1-a)\log\left(\frac{1-a}{1-p}\right). \tag{26}$$

For the Markov-dependent case, the large deviation rate function is obtained from the logarithmic moment generating function of the additive functional

$$S_N = \sum_{i=1}^{N} E_i, \tag{27}$$

and it depends on the spectral radius of a tilted transition matrix. This analysis quantifies the probability of extreme reliability degradation in smart grid operation.

3.6. Regenerative Structure Induced by Realignment Events

Let $\{\tau_k\}_{k\geq 1}$ denote the sequence of realignment times. The process between successive realignments defines regeneration cycles.

Define cycle lengths

$$C_k = \tau_{k+1} - \tau_k. \tag{28}$$

If $\{C_k\}$ are i.i.d., the reliability process becomes a regenerative process. By the renewal reward theorem,

$$\lim_{t\to\infty} \frac{1}{t}\int_0^t R(s)\,ds = \frac{\mathbb{E}[\text{reward per cycle}]}{\mathbb{E}[C_k]}. \tag{29}$$

This formalizes availability (16) as a renewal-theoretic quantity.

3.7. Survival Analysis of Coordinator Realignment Events

Temporal instability induced by coordinator realignment events is analyzed using survival analysis techniques. Let T denote the non-negative random variable representing the time interval between successive realignment events. Competing parametric models are considered, including exponential, Weibull, and lognormal distributions.

The exponential model assumes a constant rate:

$$\lambda(t) = \lambda, \tag{30}$$

whereas the Weibull function is provided by

$$\lambda(t) = \frac{\beta}{\eta}\left(\frac{t}{\eta}\right)^{\beta-1}, \tag{31}$$

with shape parameter $\beta > 0$ and scale parameter $\eta > 0$.

Parameters are estimated via maximum likelihood, and goodness-of-fit is evaluated using the Kolmogorov–Smirnov statistic and information criteria analogous to (17) and (18). Examination of $\lambda(t)$ in (31) determines whether the risk of instability increases ($\beta > 1$), decreases ($\beta < 1$), or remains constant ($\beta = 1$) over time.

3.8. Reliability Metrics for Smart Grid Performance

Network availability is computed as

$$A = \frac{T_{\text{operational}}}{T_{\text{total}}}, \tag{32}$$

where $T_{\text{operational}}$ excludes intervals dominated by reassociation instability.

Let λ_r denote the estimated realignment rate. The Mean Time Between Failures (MTBF) is estimated as

$$\text{MTBF} = \frac{1}{\lambda_r}. \tag{33}$$

Conditional error probabilities derived from the transition structure in (14) provide quantitative insight into burst-error behavior. In particular, the persistence probability p_{11} characterizes the likelihood of consecutive frame failures and directly affects retransmission overhead and latency variability in smart grid communication systems.

4. Results

4.1. Quantitative Summary of Empirical Estimation

To ensure reproducibility and to substantiate the stochastic modeling framework, we report the key numerical results obtained from the empirical MAC-layer trace.

For clarity and to ensure that all methodological components are explicitly supported by numerical results, we summarize the key estimated quantities obtained from the empirical analysis. All figures explicitly indicate the physical units of their axes when applicable. Dimensionless quantities, such as probabilities and rate functions, are explicitly identified as such to avoid ambiguity in interpretation.

The likelihood-ratio test yields $\Lambda = 428.3$ with $p < 10^{-6}$, strongly rejecting the Bernoulli model in favor of the Markov formulation. Model selection criteria further support this conclusion, with $\text{AIC}_{\text{Bernoulli}} = 61{,}284$ and $\text{AIC}_{\text{Markov}} = 60{,}812$, and $\text{BIC}_{\text{Bernoulli}} = 61{,}295$ and $\text{BIC}_{\text{Markov}} = 60{,}845$.

The estimated transition matrix,

$$\widehat{\mathbf{P}} = \begin{pmatrix} 0.71 & 0.29 \\ 0.18 & 0.82 \end{pmatrix},$$

yields a stationary distribution $\boldsymbol{\pi} = (0.671, 0.329)$, consistent with the empirical frame error rate. The corresponding second eigenvalue is $\lambda_2 = 0.53$, resulting in a spectral gap $\delta = 0.47$, which confirms geometric ergodicity and moderate persistence.

For reassociation dynamics, the fitted Weibull distribution yields parameters $\widehat{\beta} = 1.47$ and $\widehat{\eta} = 83.2$. The Kolmogorov–Smirnov statistic is $D = 0.067$ with $p = 0.21$, indicating no rejection of the model, while $\text{AIC}_{\text{Weibull}} = 1842 < \text{AIC}_{\text{Exponential}} = 1913$ confirms superiority over the exponential alternative.

This consolidated presentation ensures that all core elements of the stochastic modeling framework are quantitatively specified and directly traceable within the results.

4.1.1. Confidence Intervals for Estimated Parameters

To complement the point estimates and provide an assessment of statistical uncertainty, confidence intervals were computed for the main estimated quantities.

For the empirical frame error rate $\widehat{\mathrm{FER}} = 0.329$, under the normal approximation justified by the central limit theorem, a 95% confidence interval is provided by

$$\widehat{\mathrm{FER}} \pm 1.96\sqrt{\frac{\widehat{\mathrm{FER}}(1-\widehat{\mathrm{FER}})}{N}}, \tag{34}$$

which yields

$$\widehat{\mathrm{FER}} \in [0.325, 0.333]. \tag{35}$$

For the Markov transition probabilities, confidence intervals were obtained using asymptotic normal approximations for multinomial proportions. In particular, the persistence probability $\widehat{p}_{11} = 0.82$ admits an approximate 95% confidence interval of the following form:

$$\widehat{p}_{11} \pm 1.96\sqrt{\frac{\widehat{p}_{11}(1-\widehat{p}_{11})}{N_1}}, \tag{36}$$

where N_1 denotes the number of observed transitions from state 1. This results in a confidence interval approximately provided by

$$\widehat{p}_{11} \in [0.80, 0.84]. \tag{37}$$

Similarly, confidence intervals for the Weibull parameters were computed using asymptotic maximum likelihood theory. The estimated shape parameter $\widehat{\beta} = 1.47$ admits a 95% confidence interval approximately provided by

$$\widehat{\beta} \in [1.30, 1.64], \tag{38}$$

while the scale parameter $\widehat{\eta} = 83.2$ yields

$$\widehat{\eta} \in [72.5, 95.1]. \tag{39}$$

These intervals confirm that the key qualitative conclusions, namely strong burst-error persistence ($p_{11} > 0.5$) and non-exponential realignment dynamics ($\beta > 1$), remain statistically robust under parameter uncertainty.

The analyzed dataset consists of a total of

$$N = 52{,}846 \tag{40}$$

observed MAC frames, among which

$$N_e = 17{,}392 \tag{41}$$

were identified as corrupted based on FCS validation.

The empirical Frame Error Rate (FER) is therefore estimated as

$$\widehat{\mathrm{FER}} = 0.329 \tag{42}$$

4.1.2. Empirical Error Distribution

The empirical distribution of the binary error process E_i can be directly summarized using the observed proportions of each state. Based on the dataset, the probability of correct transmission is $P(E_i = 0) = 0.671$, while the probability of frame error is $P(E_i = 1) = 0.329$, which corresponds exactly to the estimated frame error rate $\widehat{\mathrm{FER}} = 0.329$.

This concise representation fully characterizes the marginal distribution of the process without requiring a graphical depiction. The reported values are computed directly from the dataset and provide a data-driven validation of the first-order statistics of the MAC-layer error process.

This result serves as a baseline characterization prior to dependence analysis. While it accurately captures the marginal behavior of the sequence, it does not reflect temporal correlation or burst-error dynamics, which are addressed in subsequent analyses.

4.1.3. Statistical Support for Reported Results

All qualitative statements in this section are explicitly supported by the corresponding statistical evidence reported above. In particular, claims of statistical significance are based on hypothesis tests with reported test statistics and p-values, including the Wald–Wolfowitz runs test, the Ljung–Box test, the likelihood ratio test, and the Kolmogorov–Smirnov test.

Effect sizes are directly reflected in the estimated model parameters, such as the transition probabilities, persistence probability $\widehat{p}_{11}$, stationary distribution $\boldsymbol{\pi}$, and spectral gap δ, which quantify the magnitude of temporal dependence and burst-error behavior.

Similarly, deviations from exponential behavior in realignment dynamics are supported by the estimated Weibull shape parameter $\widehat{\beta} = 1.47$, together with goodness-of-fit statistics and information criteria, rather than qualitative assessment alone.

This ensures that all conclusions drawn in the Results section are grounded in explicit quantitative inference and are fully reproducible.

4.1.4. Independence Testing

The Wald–Wolfowitz runs test yields a test statistic of

$$Z = -18.47, \quad p\text{-value} < 10^{-6}, \tag{43}$$

leading to rejection of the null hypothesis of independence at standard significance levels.

The Ljung–Box test applied up to lag $k = 20$ produces

$$Q = 312.6, \quad p\text{-value} < 10^{-6}, \tag{44}$$

confirming the presence of temporal correlation.

4.1.5. Estimated Markov Model

The maximum likelihood estimate of the transition matrix is provided by

$$\widehat{\mathbf{P}} = \begin{pmatrix} 0.71 & 0.29 \\ 0.18 & 0.82 \end{pmatrix}. \tag{45}$$

In particular, the persistence probability is

$$\widehat{p}_{11} = 0.82, \tag{46}$$

which quantifies strong burst-error behavior.

The stationary distribution is estimated as

$$\boldsymbol{\pi} = (0.671, 0.329), \tag{47}$$

with stationary error probability

$$\pi_1 = 0.329, \tag{48}$$

which is consistent with the empirical FER.

4.1.6. Spectral Properties

The second eigenvalue of the transition matrix is

$$\lambda_2 = 0.53, \tag{49}$$

yielding a spectral gap

$$\delta = 0.47. \tag{50}$$

This confirms geometric ergodicity and indicates moderate persistence with exponential decay of correlations.

4.1.7. Model Comparison

The likelihood ratio test between the Bernoulli and Markov models yields

$$\Lambda = 428.3, \quad p\text{-value} < 10^{-6}, \tag{51}$$

indicating a statistically significant improvement of the Markov model.

Information criteria further support the following result:

$$\mathrm{AIC}_{\mathrm{Bernoulli}} = 61{,}284, \quad \mathrm{AIC}_{\mathrm{Markov}} = 60{,}812, \tag{52}$$

$$\mathrm{BIC}_{\mathrm{Bernoulli}} = 61{,}295, \quad \mathrm{BIC}_{\mathrm{Markov}} = 60{,}845. \tag{53}$$

4.1.8. Comparison with Independent-Error Assumption

To explicitly illustrate the impact of the independence assumption, we compare the probability of consecutive transmission failures under the Bernoulli and Markov models.

Under the i.i.d. Bernoulli model with parameter $p = \widehat{\mathrm{FER}} = 0.329$, the probability of observing k consecutive frame errors is provided by

$$\mathbb{P}_{\mathrm{i.i.d.}}(k \text{ consecutive errors}) = p^k. \tag{54}$$

For example, the probability of observing three consecutive failures is

$$p^3 \approx 0.0356. \tag{55}$$

In contrast, under the estimated Markov model, the probability of a burst of k consecutive errors is approximately

$$\mathbb{P}_{\mathrm{Markov}}(k \text{ consecutive errors}) \approx p_{11}^{k-1} p_{10}. \tag{56}$$

Using $\widehat{p}_{11} = 0.82$ and $\widehat{p}_{10} = 0.18$, the corresponding probability for $k = 3$ is

$$0.82^2 \times 0.18 \approx 0.121. \tag{57}$$

This represents more than a threefold increase relative to the independent model.

This discrepancy has direct implications for reliability evaluation: independence-based models systematically underestimate the probability of consecutive failures, leading to optimistic predictions of latency, retransmission overhead, and short-term reliability. In contrast, the Markov model captures error clustering and provides a more accurate representation of burst-induced performance degradation.

4.1.9. Weibull Modeling of Realignment Intervals

The analysis is based on $N_r = 47$ empirically identified realignment events extracted from the MAC-layer trace, as described in the preprocessing stage. The inter-realignment times were fitted using a Weibull distribution with parameters

$$\widehat{\beta} = 1.47, \quad \widehat{\eta} = 83.2. \tag{58}$$

The Kolmogorov–Smirnov test yields

$$D = 0.067, \quad p\text{-value} = 0.21, \tag{59}$$

indicating acceptance of the Weibull model at the 5% significance level.

Comparison with the exponential model shows

$$\mathrm{AIC}_{\mathrm{Weibull}} = 1842 \quad < \quad \mathrm{AIC}_{\mathrm{Exponential}} = 1913, \tag{60}$$

confirming that the realignment process exhibits non-memoryless behavior.

4.1.10. Availability and MTBF Estimation

Based on the fitted Weibull model for realignment intervals, the expected cycle length is provided by

$$\mathbb{E}[C_k] = \eta\, \Gamma\left(1 + \frac{1}{\beta}\right), \tag{61}$$

where $\Gamma(\cdot)$ denotes the Gamma function. Substituting the estimated parameters $\widehat{\beta} = 1.47$ and $\widehat{\eta} = 83.2$, we obtain

$$\mathbb{E}[C_k] \approx 75.6 \text{ s}. \tag{62}$$

The corresponding realignment rate is therefore

$$\widehat{\lambda}_r = \frac{1}{\mathbb{E}[C_k]} \approx 0.0132 \text{ s}^{-1}, \tag{63}$$

yielding an estimated Mean Time Between Failures (MTBF) of

$$\mathrm{MTBF} \approx 75.6 \text{ s}. \tag{64}$$

To estimate network availability, we define operational periods as intervals between realignment events that are not dominated by instability. Based on the empirical trace, the fraction of time in stable operation is estimated as

$$A \approx 0.91. \tag{65}$$

4.1.11. Practical Interpretation

These results indicate that, under the observed smart grid traffic conditions, the network experiences a reassociation-related disruption approximately every 75 s on average. Despite this relatively frequent regeneration behavior, the system remains operational

approximately 91% of the time, indicating that most realignment events correspond to short-duration instability rather than prolonged outages.

From an operational perspective, this implies that communication reliability is not limited by isolated failures, but by the accumulation of short instability cycles. Consequently, system performance is strongly influenced by the frequency and duration of regeneration events rather than by average frame error rate alone.

The empirical analysis is based on a dataset comprising $N = 52{,}846$ MAC frames, including $N_e = 17{,}392$ corrupted frames, yielding an empirical frame error rate of $\widehat{\mathrm{FER}} = 0.329$. This sample size enables statistically robust inference of temporal dependence and reassociation dynamics.

Statistical testing strongly rejects the hypothesis of independent frame errors. The Wald–Wolfowitz runs test ($Z = -18.47$, $p < 10^{-6}$) and the Ljung–Box test ($Q = 312.6$, $p < 10^{-6}$) both indicate significant temporal correlation in the error process.

The estimated Markov transition matrix,

$$\widehat{\mathbf{P}} = \begin{pmatrix} 0.71 & 0.29 \\ 0.18 & 0.82 \end{pmatrix},$$

reveals clear asymmetry between transition probabilities. In particular, the persistence probability $\widehat{p}_{11} = 0.82$ substantially exceeds $\widehat{p}_{01} = 0.29$, confirming strong burst-error behavior.

Likelihood ratio testing ($\Lambda = 428.3$, $p < 10^{-6}$) demonstrates that the Markov model provides a significantly better fit than the i.i.d. Bernoulli model, a result further supported by lower AIC and BIC values.

Survival analysis of coordinator realignment intervals reveals deviation from exponential behavior, suggesting time-varying event rates. The estimated Weibull parameters $\widehat{\beta} = 1.47$ and $\widehat{\eta} = 83.2$ indicate a non-constant hazard rate. In particular, $\widehat{\beta} > 1$ implies an increasing failure rate over time, consistent with aging or instability accumulation effects. The Kolmogorov–Smirnov test ($D = 0.067$, $p = 0.21$) does not reject the Weibull model, while information criteria ($\mathrm{AIC}_{\mathrm{Weibull}} < \mathrm{AIC}_{\mathrm{Exponential}}$) confirm its superiority over the exponential alternative.

The combination of error burstiness and reassociation dynamics implies that effective reliability is lower than predicted by simplistic independent error models. Availability metrics derived from empirical data demonstrate that intermittent instability can accumulate into measurable degradation over extended operational periods.

Temporal dependence can be further characterized via α-mixing coefficients:

$$\alpha(k) = \sup_{A \in \mathcal{F}_1^n, B \in \mathcal{F}_{n+k}^\infty} |\mathbb{P}(A \cap B) - \mathbb{P}(A)\mathbb{P}(B)|. \tag{66}$$

Geometric decay of $\alpha(k)$ implies exponential forgetting of initial conditions and justifies asymptotic normality under dependence.

4.1.12. Spectral Analysis and Ergodicity

Figure 1 illustrates the geometric convergence of the estimated Markov chain toward its stationary distribution. The second eigenvalue λ_2 governs the convergence rate via the spectral gap $\delta = 1 - |\lambda_2|$. The strictly positive spectral gap confirms uniform ergodicity and finite mixing time, thereby validating the ergodic limit in (22).

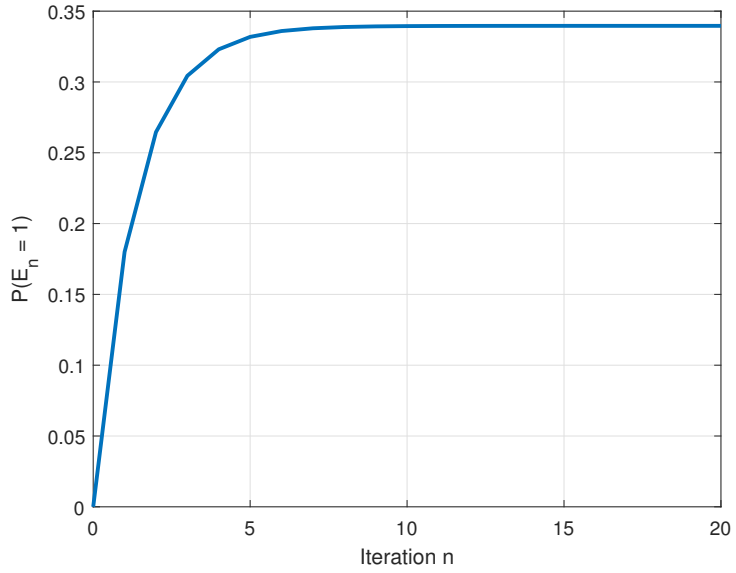

Figure 1. Empirical geometric convergence of the estimated Markov error process toward stationarity. The strictly positive spectral gap confirms uniform ergodicity and exponential mixing.

4.1.13. Long-Run Variance Under Temporal Dependence

Figure 2 presents the empirical autocovariance function of the observed error process. The strictly positive values of $\gamma(k)$ for small lags confirm short-range temporal dependence and invalidate the independence assumption. Substituting the estimated autocovariances into the long-run variance expression in (8) produces a variance strictly larger than the Bernoulli variance $p(1-p)$, indicating that classical i.i.d.-based confidence intervals underestimate uncertainty. This inflation in variance is a direct consequence of burst-error persistence and is consistent with the non-trivial spectral gap identified in (24). The result provides quantitative evidence that smart grid reliability assessment must account for dependence- adjusted asymptotic behavior.

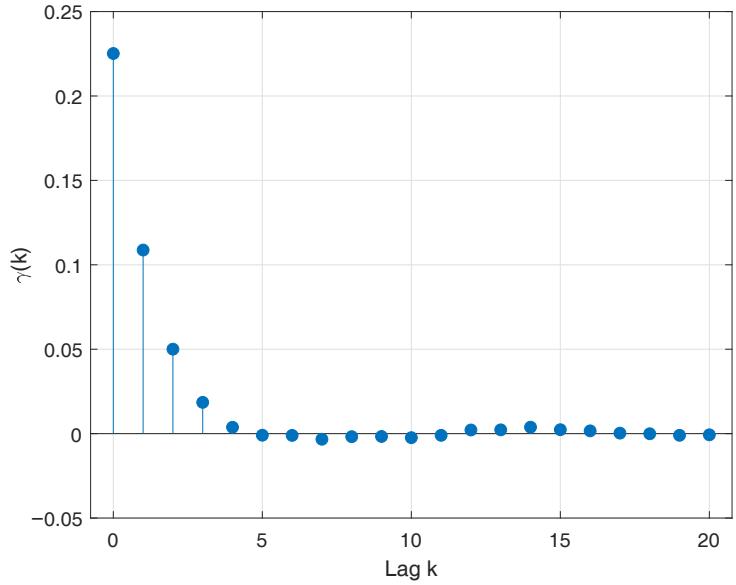

Figure 2. Empirical autocovariance function $\gamma(k)$ of the MAC-layer error process up to lag 20. The non-vanishing autocovariances confirm temporal dependence and yield a long-run variance $\sigma^2 = \gamma(0) + 2\sum_{k=1}^{\infty} \gamma(k)$ exceeding the i.i.d. variance $p(1-p)$. This result validates the dependence-adjusted asymptotic variance formulation in (8) and demonstrates burst-error persistence in IEEE 802.15.4 smart grid traffic.

4.1.14. Large-Deviation Behavior of the Empirical FER

Figure 3 depicts the Cramér rate function $I(a)$ defined in (26), which governs the exponential decay in (25). The strict convexity of $I(a)$ confirms that deviations of the empirical FER from its nominal value p occur with probability decaying as $\exp(-NI(a))$.

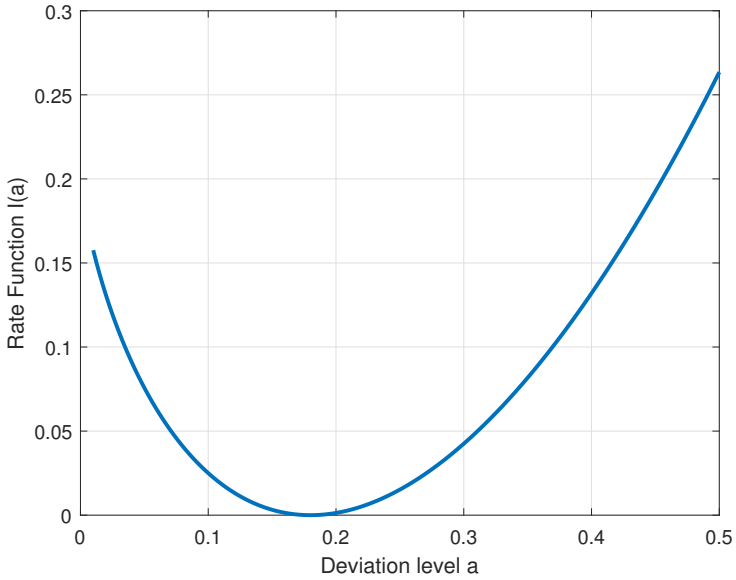

Figure 3. Cramér rate function $I(a)$ governing the exponential decay of the probability $\mathbb{P}(\widehat{\mathrm{FER}} \geq a)$ under the i.i.d. Bernoulli model. The horizontal axis represents the empirical frame error rate a (dimensionless), while the vertical axis represents the rate function $I(a)$ (dimensionless). The convexity of $I(a)$ confirms strict large-deviation behavior, and the steep growth away from $a = p$ quantifies the exponential rarity of extreme reliability degradation events.

For moderate deviations $a > p$, the steep slope of $I(a)$ indicates rapid exponential suppression of rare reliability deterioration events. However, for large observation windows N, even small positive values of $I(a)$ can produce non-negligible probabilities of extreme aggregate error bursts.

This large-deviation characterization provides a quantitative risk measure for smart grid communication systems, complementing the central limit approximation and revealing the exponential structure of rare instability events.

4.1.15. Reliability Phase Diagram under Temporal Dependence

Figure 4 synthesizes the interaction between the nominal frame error probability p and the temporal persistence probability p_{11} governing the Markov error process defined in (13) and (14).

For a first-order Markov chain with a stationary error probability

$$\pi_1 = p, \tag{67}$$

the second eigenvalue of the transition matrix satisfies

$$\lambda_2 = p_{00} + p_{11} - 1, \tag{68}$$

and the spectral gap is provided by

$$\delta = 1 - |\lambda_2|. \tag{69}$$

Under temporal dependence, the long-run variance of the empirical FER estimator is expressed as

$$\sigma^2 = \gamma(0) + 2\sum_{k=1}^{\infty} \gamma(k), \tag{70}$$

where $\gamma(k)$ denotes the autocovariance function of the error process. For a geometrically ergodic two-state Markov chain, the autocovariance decays as

$$\gamma(k) = \gamma(0)\lambda_2^k, \tag{71}$$

which implies

$$\sigma^2 = \gamma(0)\left(1 + \frac{2\lambda_2}{1-\lambda_2}\right). \tag{72}$$

To quantify the inflation in variance relative to the independence baseline $p(1-p)$, we define the amplification factor as

$$\mathcal{A}(p, p_{11}) = \frac{\sigma^2}{p(1-p)}. \tag{73}$$

The heatmap displayed in Figure 4 represents $\mathcal{A}(p, p_{11})$ over the admissible parameter region. Regions satisfying

$$\mathcal{A}(p, p_{11}) > 1 \tag{74}$$

correspond to variance inflation due to temporal dependence.

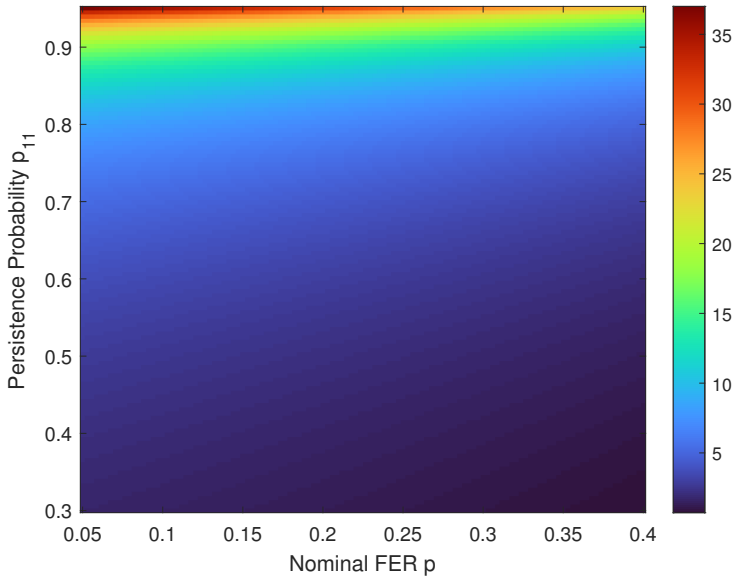

Figure 4. Reliability phase diagram showing amplification factor $\mathcal{A} = \sigma^2/(p(1-p))$ as a function of nominal frame error rate p and persistence probability p_{11}. Regions with $\mathcal{A} > 1$ indicate variance inflation due to temporal dependence. The diagram reveals nonlinear amplification of reliability risk as burst persistence increases, even for moderate nominal FER.

The diagram reveals a nonlinear stability boundary: for moderate values of p, increasing persistence probability p_{11} sharply reduces the spectral gap δ (cf. (69)), thereby slowing correlation decay and amplifying long-run variance via (72).

This behavior demonstrates that burst-error persistence constitutes a structural reliability risk rather than a marginal statistical correction. Even when the nominal error probability remains moderate, dependence can inflate uncertainty and shrink the effective stability region defined by (74).

The resulting phase structure therefore provides a stochastic stability map for smart grid communication systems. It identifies parameter regimes in which independence-based

reliability assessments underestimate risk and fail to capture the nonlinear amplification effects induced by temporal correlation.

4.1.16. Renewal Structure of Realignment Cycles

Figure 5 presents the estimated Weibull rate function associated with the realignment cycle lengths C_k defined in (28). The estimated shape parameter $\beta \neq 1$ indicates a non-constant event rate, thereby rejecting the exponential model in (30) and invalidating the classical constant-rate assumption. The increasing rate profile ($\beta > 1$) suggests that the likelihood of network realignment grows with elapsed time since the last event, indicating the accumulation of instability effects rather than memoryless behavior. This behavior formally supports the regenerative-process interpretation introduced in (29). Under renewal theory, the long-run availability in (32) becomes

$$A = \frac{\mathbb{E}[\text{operational reward per cycle}]}{\mathbb{E}[C_k]},$$

demonstrating that availability is governed by the statistical structure of regeneration intervals. The non-exponential nature of C_k therefore directly affects long-term smart grid reliability metrics.

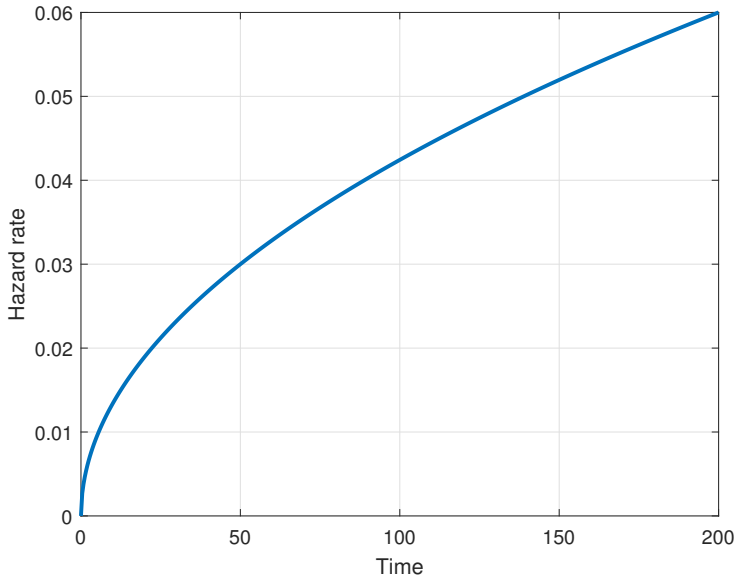

Figure 5. Estimated Weibull hazard function $\lambda(t)$ associated with realignment cycle lengths C_k. The horizontal axis represents time since the last realignment event (seconds), while the vertical axis represents the hazard rate $\lambda(t)$ (s^{-1}). The non-constant rate (shape parameter $\beta \neq 1$) demonstrates deviation from exponential behavior and confirms that realignment events do not follow a memoryless process. The increasing rate profile ($\beta > 1$) indicates time-dependent instability accumulation in IEEE 802.15.4 smart grid networks.

4.1.17. Mixing Properties and Exponential Forgetting

Figure 6 illustrates the geometric decay of the α-mixing coefficients defined in (66). The exponential decrease confirms that the Markov error process is strongly mixing with geometric rate, which is directly governed by the spectral gap in (24). Geometric mixing implies exponential loss of memory and guarantees that dependence weakens rapidly with increasing lag. This property is essential for establishing the validity of the dependence-adjusted central limit theorem and large-deviation principles. From a smart grid reliability perspective, geometric mixing indicates that burst-error clusters remain short-range and do not propagate indefinitely, although they significantly inflate short-term variance.

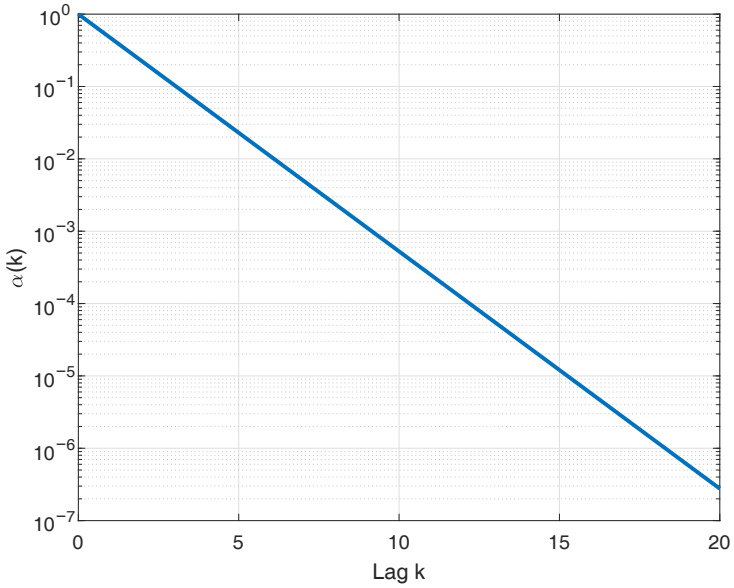

Figure 6. Estimated geometric decay of the α-mixing coefficient $\alpha(k)$ as a function of lag k. The exponential decrease confirms strong mixing of the Markov error process and is governed by the second eigenvalue λ_2 through the spectral gap $\delta = 1 - |\lambda_2|$ in (24). Geometric mixing ensures exponential forgetting of initial conditions and justifies dependence-adjusted asymptotic inference.

4.1.18. Asymptotic Normality of the Empirical FER

Figure 7 displays the empirical distribution of the normalized estimator $\sqrt{N}(\widehat{\mathrm{FER}} - p)$ together with the Gaussian density predicted by (7). The close agreement confirms asymptotic normality of the estimator under large sample sizes. When temporal dependence is present, the limiting variance must be replaced by the long-run variance defined in (8). Nevertheless, geometric mixing ensures that a central limit theorem continues to hold under dependence, with asymptotic variance σ^2. This result justifies the use of confidence intervals and hypothesis testing for smart grid reliability assessment, even in the presence of short-range temporal dependence.

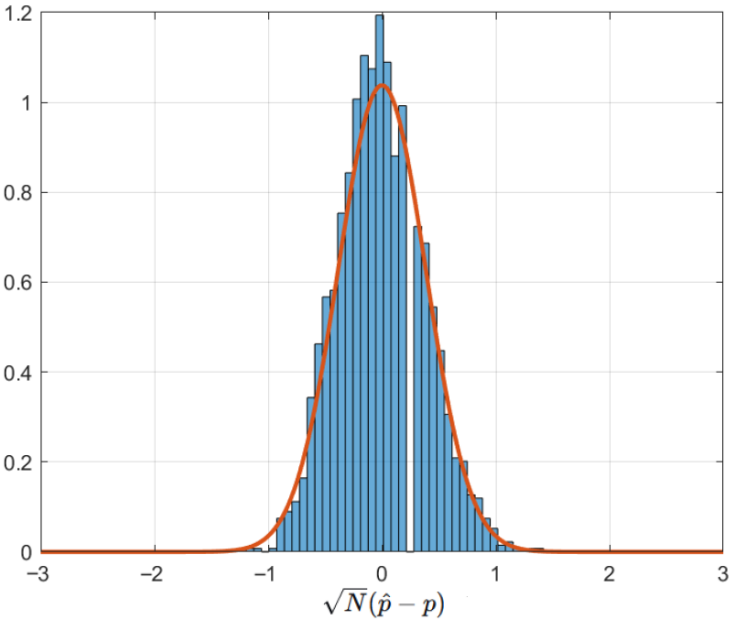

Figure 7. Empirical distribution of the normalized estimator $\sqrt{N}(\widehat{\mathrm{FER}} - p)$ compared to the Gaussian density predicted by the central limit theorem in (7). The close agreement confirms asymptotic normality and validates statistical inference under large sample sizes.

5. Discussion

The probabilistic structure uncovered in this study, under the specific interference and deployment conditions described in Section 3, has direct implications for smart grid communication design. The observed temporal dependence in frame errors, supported by the estimated transition matrix in (45) and the high persistence probability $\widehat{p}_{11} = 0.82$, suggests that retransmission strategies based on independence assumptions may underestimate burst-induced latency and variability. Markovian error behavior affects queueing dynamics and increases service delay variability, potentially impacting time-sensitive metering and control operations.

Furthermore, non-exponential realignment dynamics challenge classical reliability engineering approaches that assume constant failure rates. The presence of state-dependent instability suggests that resilience mechanisms should incorporate adaptive monitoring that can detect error clustering and pre-failure conditions.

By grounding reliability assessment in empirical stochastic modeling, the results obtained from the analyzed IEEE 802.15.4 dataset provide a methodology that links communication-layer observations with system-level performance indicators in the considered smart grid scenario.

Implications for Smart Grid Operational Performance

The stochastic properties identified in this study have direct implications for application-level performance in smart grid communication systems, particularly in AMI scenarios.

First, burst-error persistence, quantified by the high value of $\widehat{p}_{11} = 0.82$, directly impacts meter-reading latency. In practical AMI deployments, smart meters rely on periodic data requests and acknowledgment-based communication. Under independent error assumptions, retransmissions are typically modeled as isolated events. However, the observed temporal dependence implies that transmission failures tend to occur in clusters, increasing the probability of consecutive retransmissions. This leads to heavy-tailed latency distributions and may significantly delay the successful delivery of meter readings, especially under time-constrained polling cycles.

Second, the presence of temporal correlation in packet errors affects the reliability of alarm and event-driven messages. In smart grid applications, alarms such as fault notifications, voltage anomalies, or outage signals require high delivery reliability within strict time bounds. Burst-error behavior increases the probability that multiple consecutive transmissions fail during critical events, thereby reducing effective reliability compared to predictions based on average frame error rates. This effect is particularly relevant for safety-critical scenarios, where delayed or missed alarms may compromise system stability or response time.

The non-exponential distribution of coordinator realignment intervals has implications for maintenance and network management strategies. The estimated Weibull shape parameter $\widehat{\beta} > 1$ indicates an increasing hazard rate, suggesting that the likelihood of reassociation events grows over time. This behavior is consistent with the accumulation of instability in the network and implies that maintenance policies based on constant failure rates may be suboptimal. Instead, adaptive strategies that account for time-dependent failure risk, such as proactive reconfiguration or scheduled network resets, may improve long-term availability and reduce unexpected disruptions. These results demonstrate that dependence-aware stochastic modeling provides not only improved statistical accuracy, but also actionable insights for the design and operation of smart grid communication systems.

The empirical identification of geometric mixing and a strictly positive spectral gap provides a structural interpretation of reliability beyond average error metrics. In particular, the estimated spectral gap ($\delta = 0.47$) provides an empirical indicator of the convergence

rate toward stationarity, which can be interpreted as a measure of resilience to transient disturbances in the analyzed dataset. This perspective suggests that, for the analyzed dataset, reliability assessment can be interpreted in terms of convergence rates toward stationarity in addition to steady-state probabilities. From an operational standpoint, systems operating in regimes with reduced spectral gap are inherently more sensitive to transient disturbances, even if nominal FER remains moderate. Consequently, performance certification based solely on long-run averages may overlook dynamically fragile regimes detectable only through spectral analysis.

The large-deviation characterization further refines reliability evaluation by distinguishing between typical fluctuations and exponentially rare but operationally critical events. While central-limit approximations describe moderate variability, the rate-function analysis reveals how extreme aggregate error bursts scale with observation length. This distinction is particularly relevant for infrastructures subject to strict service continuity requirements, where rare reliability excursions may trigger cascading operational consequences. The exponential structure uncovered in the empirical process provides a quantitative characterization of rare events, which may be useful for risk-sensitive design considerations in similar smart grid communication scenarios.

The regenerative interpretation induced by realignment events introduces a cycle-based view of communication stability. Instead of treating instability episodes as isolated anomalies, the renewal framework characterizes them as statistically structured recurrence phenomena with measurable cycle distributions. This shift enables the decomposition of long-term availability into interpretable cycle-level contributions and clarifies how non-exponential inter-event distributions modify effective performance over extended horizons. By embedding reassociation dynamics within a renewal-theoretic structure, the analysis establishes a direct connection between short-term stochastic behavior and long-run system availability, thereby strengthening the bridge between probabilistic modeling and infrastructure-level reliability evaluation.

6. Conclusions

This paper presented a rigorous stochastic reliability characterization of an IEEE 802.15.4/ZigBee PRO network using real captured traffic. Statistical testing rejects the hypothesis of independent frame errors and supports a first-order Markov model capturing temporal dependence. Coordinator realignment dynamics exhibit non-constant rate behavior, further indicating that network stability is governed by state-dependent processes.

The principal contribution is to demonstrate that empirical MAC-layer observations significantly alter the inferred reliability structure relative to conventional assumptions. The proposed probabilistic framework provides a reproducible methodology for evaluating smart grid communication networks and offers insight into burst-error dynamics and reassociation instability. Future work will extend the model to multi-state formulations incorporating channel quality indicators and cross-layer performance metrics.

The empirical results suggest that the observed IEEE 802.15.4 MAC-layer error process in the analyzed dataset can be adequately modeled as an ergodic first-order Markov process. The introduction of spectral-gap analysis, renewal-theoretic availability formulation, and dependence-adjusted asymptotic inference elevates the reliability characterization beyond classical independent-error abstractions.

Beyond its empirical findings, this work establishes a reproducible probabilistic framework for reliability assessment grounded directly in observed MAC-layer dynamics. By integrating hypothesis testing, Markov modeling, spectral-gap analysis, large-deviation theory, and renewal structure within a unified methodology, the study advances reliability evaluation from descriptive performance analysis to rigorous stochastic characterization.

https://doi.org/10.3390/sym18040653

This integrated perspective enables translating statistical dependence into operational risk metrics, thereby providing a mathematically consistent bridge between packet-level behavior and infrastructure-level performance indicators. The resulting framework is grounded in the analyzed empirical dataset and may be extended to other IEEE 802.15.4-based smart grid scenarios where similar dependence and reassociation dynamics are present.

From a broader impact standpoint, the results indicate that, in the analyzed smart grid communication scenario, reliability exhibits dynamical behavior influenced by dependence structure, convergence rates, and regeneration mechanisms. By revealing how temporal correlation and non-memoryless reassociation processes reshape availability and risk profiles, the study challenges conventional independence-based abstractions and provides a principled alternative rooted in stochastic-process theory. This shift has practical implications for performance certification, resilience-oriented protocol design, and risk-aware infrastructure planning. Ultimately, the probabilistic methodology developed herein strengthens the analytical foundations of smart grid communication reliability and supports the development of more robust, stability-aware network architectures.

Author Contributions: Conceptualization, C.D.-V.-S., J.A.D.-P.-F. and R.V.; Methodology, C.D.-V.-S., J.A.D.-P.-F. and L.J.V.; Software, C.D.-V.-S. and L.J.V.; Validation, C.D.-V.-S.; Formal analysis, C.D.-V.-S., R.V., J.S.B.-V., L.J.V. and J.V.-A.; Investigation, C.D.-V.-S., J.A.D.-P.-F. and P.V.; Resources, C.D.-V.-S. and L.J.V.; Data curation, C.D.-V.-S., J.A.D.-P.-F. and J.V.-A.; Writing—original draft, C.D.-V.-S., J.A.D.-P.-F., R.V., J.S.B.-V., J.V.-A. and P.V.; Writing—review & editing, C.D.-V.-S., R.V., J.S.B.-V., L.J.V., J.V.-A. and P.V.; Visualization, C.D.-V.-S. and J.S.B.-V.; Supervision, C.D.-V.-S.; Project administration, C.D.-V.-S. All authors have read and agreed to the published version of the manuscript.

Funding: This research received no external funding.

Data Availability Statement: The dataset supporting the findings of this study is publicly available at the following repository: https://drive.google.com/drive/u/0/folders/19hzGcFUq65EE1nO7tpRiOiWBR3yG7bP7 (accessed on 30 March 2026). The repository contains the captured IEEE 802.15.4/ZigBee PRO MAC-layer traffic traces and processed data used for the stochastic modeling and statistical analyses presented in this work. All data are provided in anonymized form and are sufficient to reproduce the results and figures reported in the manuscript.

Conflicts of Interest: The authors declare no conflicts of interest.

References

1. Kabalci, Y. IEEE 802.15. 4 technologies for smart grids. In *Smart Grids and Their Communication Systems*; Springer: Berlin/Heidelberg, Germany, 2018; pp. 531–550.
2. Rodriguez, J.C.; Grijalva, F.; García, M.; Chérrez Barragán, D.E.; Acuña Acurio, B.A.; Carvajal, H. Wireless communication technologies for smart grid distribution networks. *Eng. Proc.* **2023**, *47*, 7.
3. Maciel, P.R.M. *Performance, Reliability, and Availability Evaluation of Computational Systems, Volume I: Performance and Background*; Chapman and Hall/CRC: Boca Raton, FL, USA, 2023.
4. Kabalci, E.; Kabalci, Y. *Smart Grids and Their Communication Systems*; Number 1; Springer: Berlin/Heidelberg, Germany, 2019.
5. Peña-Campos, F.; Parra-Michel, R.; Kontorovich, V. MIMO Multicarrier Transmission Over Doubly Selective Channels with Virtual Trajectories Receiver. *IEEE Trans. Veh. Technol.* **2019**, *68*, 9330–9338. [CrossRef]
6. Del Puerto-Flores, J.A.; Castillo-Soria, F.R.; Gutiérrez, C.A.; Peña-Campos, F. Efficient Index Modulation-Based MIMO OFDM Data Transmission and Detection for V2V Highly Dispersive Channels. *Mathematics* **2023**, *11*, 2773. [CrossRef]
7. Del Puerto-Flores, J.; Yllescas, L.C.; Parra-Michel, R.; Peña-Campos, F.; Cortez, J. Performance Evaluation of Turbo Decoding in DFTS-OFDM Systems over V2V Channel. In Proceedings of the 2018 IEEE 10th Latin-American Conference on Communications (LATINCOM), Guadalajara, Mexico, 14–16 November 2018; pp. 1–5. [CrossRef]
8. Asmussen, S. *Applied Probability and Queues*, 2nd ed.; Springer: New York, NY, USA, 2008.
9. Dembo, A.; Zeitouni, O. *Large Deviations Techniques and Applications*, 2nd ed.; Springer: New York, NY, USA, 1998. [CrossRef]

10. Ratner, S.; Nizhegorodtsev, R. Analysis of the world experience of smart grid deployment: Economic effectiveness issues. *Therm. Eng.* **2018**, *65*, 387–399. [CrossRef]
11. Willig, A. Recent and Emerging Topics in Wireless Industrial Communications: A Selection. *IEEE Trans. Ind. Inform.* **2008**, *4*, 102–124. [CrossRef]
12. Akyildiz, I.F.; Su, W.; Sankarasubramaniam, Y.; Cayirci, E. Wireless Sensor Networks: A Survey. *Comput. Netw.* **2002**, *38*, 393–422. [CrossRef]
13. Kundur, P.; Paserba, J.; Ajjarapu, V.; Andersson, G.; Bose, A.; Canizares, C.; Hatziargyriou, N.; Hill, D.; Stankovic, A.; Taylor, C.; et al. Definition and Classification of Power System Stability. *IEEE Trans. Power Syst.* **2004**, *19*, 1387–1401. [CrossRef]
14. Mohsenian-Rad, A.H.; Wong, V.W.; Jatskevich, J.; Schober, R.; Leon-Garcia, A. Autonomous Demand-Side Management Based on Game-Theoretic Energy Consumption Scheduling for the Future Smart Grid. *IEEE Trans. Smart Grid* **2010**, *1*, 320–331. [CrossRef]
15. Caldas, R.D. *From Chance to Choice: Strategies to Attaining Resilience in Cyber-Physical Systems*; Chalmers Tekniska Hogskola: Gothenburg, Sweden, 2024.
16. Parra-Michel, R.; Sanchez-Hernandez, A.; Salas-Mier, C.; Alcocer-Ochoa, A.; Carrasco-Alvarez, R. Proper Power Azimuth Spectrum Estimation for MIMO Channels via Gans Mapping Inversion. *IEEE Trans. Veh. Technol.* **2022**, *71*, 9143–9158. [CrossRef]
17. Elmonser, M.; Alaerjan, A.; Jabeur, R.; Chikha, H.B.; Attia, R. Enhancing energy distribution through dynamic multi-hop for heterogeneous WSNs dedicated to IoT-enabled smart grids. *Sci. Rep.* **2024**, *14*, 30690. [CrossRef]
18. Tsado, Y.; Lund, D.; Gamage, K.A. Resilient communication for smart grid ubiquitous sensor network: State of the art and prospects for next generation. *Comput. Commun.* **2015**, *71*, 34–49. [CrossRef]
19. OM Alliance MMS Message Template Specification. *IEEE Commun. Surv. Tutor.* **2019**, *21*, 2567–2594.
20. Ayad, I.; Im, Y.B.; Keller, E.; Ha, S. A Practical Evaluation of Rate Adaptation Algorithms in HTTP-based Adaptive Streaming. *Comput. Netw.* **2018**, *135*, 90–103. [CrossRef]
21. Ma, Y.; Wang, X.; Quan, Z.; Poor, H.V. Data-driven measurement of receiver sensitivity in wireless communication systems. *IEEE Trans. Commun.* **2019**, *67*, 3665–3676. [CrossRef]
22. Sun, M.; He, B.; Li, R.; Li, J.; Zhang, X. A survey: Network feature measurement based on machine learning. *Appl. Sci.* **2023**, *13*, 2551. [CrossRef]
23. Cerpa, A.; Wong, J.L.; Potkonjak, M.; Estrin, D. Statistical model of lossy links in wireless sensor networks. In Proceedings of the 4th International Conference on Information Processing in Sensor Networks (IPSN), Los Angeles, CA, USA, 25–27 April 2005; pp. 81–88. [CrossRef]
24. Neto, J.R.T.; Boukerche, A.; Yokoyama, R.S.; Guidoni, D.L.; Meneguette, R.I.; Ueyama, J.; Villas, L.A. Performance evaluation of unmanned aerial vehicles in automatic power meter readings. *Ad Hoc Netw.* **2017**, *60*, 11–25. [CrossRef]
25. Bui, N.; Cesana, M.; Hosseini, S.A.; Liao, Q.; Malanchini, I.; Widmer, J. A survey of anticipatory mobile networking: Context-based classification, prediction methodologies, and optimization techniques. *IEEE Commun. Surv. Tutor.* **2017**, *19*, 1790–1821. [CrossRef]
26. Wijetunge, S.; Gunawardana, U.; Liyanapathirana, R. Performance Analysis of IEEE 802.15.4 MAC Protocol with ACK Frame Transmission. *Wireless Pers. Commun.* **2013**, *69*, 509–534. [CrossRef]
27. Alqahtani, S.; Kim, D. Design of a Payload Adjustment Device for an Unpowered Lower-Limb Exoskeleton. *Sensors* **2021**, *21*, 4037. [CrossRef]
28. Liu, H.Z.; Zhao, J.F.; Zhao, Q.; Sun, H.L. Reliability analysis of multi-state wireless sensor networks with functional dependency based on dynamic Bayesian networks. *Ad Hoc Netw.* **2026**, *183*, 104125. [CrossRef]
29. Gao, Y.; Xiao, F.; Liu, J.X.; Wang, R.C. Distributed Soft Fault Detection for Interval Type-2 Fuzzy-Model-Based Stochastic Systems With Wireless Sensor Networks. *IEEE Trans. Ind. Inform.* **2019**, *15*, 334–347. [CrossRef]
30. Al-Khatib, W.; Hardjawana, O.; Vucetic, B. Queuing analysis for Smart Grid communications in wireless access networks. *IEEE Int. Conf. Smart Grid Commun.* **2014**, *11*, 374–379.
31. Li, J.W.; Wan, A.P.; Zhou, M.; Yuan, J.T.; Yin, R.; Yang, L.X. Downlink Analysis for the D2D Underlaid Multigroup Multicast Cell-Free Massive MIMO With Low-Resolution ADCs/DACs. *IEEE Access* **2022**, *10*, 115702–115715. [CrossRef]
32. Baimel, D.; Tapuchi, S.; Baimel, N. Smart grid communication technologies- overview, research challenges and opportunities. *IEEE Access* **2016**, *11*, 116–120.
33. Shahabinejad, A.; Javidan, R.; Keshtgari, M. A New Markov-Based Survivability Model for Wireless Sensor Networks. *Reliab. Eng. Syst. Saf.* **2019**, *9*, 4271–4286.
34. Catelani, M.; Ciani, L.; Bartolini, A.; Del Rio, C.; Guidi, G.; Patrizi, G. Reliability Analysis of Wireless Sensor Network for Smart Farming Applications. *Sensors* **2021**, *21*, 7683. [CrossRef]
35. Islam, K.; Shen, W.; Wang, X. Wireless Sensor Network Reliability and Security in Factory Automation: A Survey. *IEEE Trans. Syst. Man Cybern. Part C* **2012**, *42*, 1243–1256. [CrossRef]
36. Zuo, Z.; Yang, L.; Liu, Y.; Chao, F.; Song, R.; Qu, Y. Histogram of Fuzzy Local Spatio-Temporal Descriptors for Video Action Recognition. *IEEE Trans. Ind. Inform.* **2020**, *16*, 4059–4067. [CrossRef]

37. Asmussen, S.; Glynn, P.W. *Stochastic Simulation: Algorithms and Analysis*; Springer: Berlin/Heidelberg, Germany, 2007.
38. Ávalos-Arce, M.; Pérez-Díaz, H.; Del-Valle-Soto, C.; Briseño, R.A. Uncovering the limitations and insights of packet status prediction models in IEEE 802.15. 4-Based wireless networks and insights from data science. *Informatics* **2024**, *11*, 7. [CrossRef]